청정에너지기술

Effects of Mg Addition to Cu/Al$_2$O$_3$ Catalyst for Low-Temperature Water Gas Shift (LT-WGS) Reaction

Zakia Akter Sonia[1], Ji Hye Park[2], Wathone Oo[1], and Kwang Bok Yi[2]*

[1]Graduate School of Energy Science and Technology, Chungnam National University
99 Daehak-ro, Yuseong-gu, Daejeon 34134, South Korea
[2]Department of Chemical Engineering Education, Chungnam National University
99 Daehak-ro, Yuseong-gu, Daejeon 34134, South Korea

Abstract

To investigate the effects of Mg addition at different aging times and temperatures, Cu/MgO/Al$_2$O$_3$ catalysts were synthesized for the low-temperature water gas shift (LT-WGS) reaction. The co-precipitation method was employed to prepare the catalysts with a fixed Cu amount of 30 mol% and varied amounts of Mg/Al. Synthesized catalysts were characterized using XRD, BET, and H$_2$-TPR analysis. Among the prepared catalysts, the highest CO conversion was achieved by the Cu/MgO/Al$_2$O$_3$ catalyst (30/40/30 mol%) with a 60 °C aging temperature and a 24 h aging time under a CO$_2$-rich feed gas. Due to it having the lowest reduction temperature and a good dispersion of CuO, the catalyst exhibited around 65% CO conversion with a gas hourly space velocity (GHSV) of 14,089 h^{-1} at 300 °C. However, it has been noted that aging temperatures greater or less than 60 °C and aging times longer than 24 h had an adverse impact, resulting in a lower surface area and a higher reduction temperature bulk-CuO phase, leading to lower catalytic activity. The main findings of this study confirmed that one of the main factors determining catalytic activity is the ease of reducibility in the absence of bulk-like CuO species. Finally, the long-term test revealed that the catalytic activity and stability remained constant under a high concentration of CO$_2$ in the feed gas for 19 h with an average CO conversion of 61.83%.

Keywords : Petroleum cokes, Water gas shift, Catalyst, Cu/MgO/Al$_2$O$_3$, CO conversion

1. Introduction

Due to environmental issues and the depletion caused by fossil fuels, many experts believe that the energy system of the 21st century will be based on hydrogen [1]. The demand for hydrogen in South Korea is expected to surpass 1.9 M tons yr^{-1} by 2030 and 5.2 M tons yr^{-1} by 2040 [2]. According to the production method, hydrogen is classified into green, blue, and gray hydrogen [3-6]. The process of producing hydrogen should shift to favor green hydrogen in the long term. However, it should be noted that the process of electrolysis is the main cost of green hydrogen production [7-9]. Furthermore, using green hydrogen is difficult due to economic and technological limitations. Therefore, as a realistic alternative, it is crucial to increase the production and use of blue hydrogen [10]. In particular, to explain the petroleum coke (pet coke) gasification process, blue hydrogen can produce hydrogen in

significant quantities by applying existing infrastructure and technology and converting it into syngas by utilizing pet coke, waste, etc. [11]. Consequently, producing high-value syngas through the gasification of pet coke is an effective and promising technology for satisfying the demand for hydrogen. Pet coke gasification produces syngas with a typical average composition of around 47.72 % CO, 30.33 % H$_2$, 17.88 % CO$_2$, and a small concentration of other gases [12-14].

In general, water gas shift (WGS) reaction is employed to produce high-purity hydrogen from the excess CO in the pet coke-derived syngas [15,16]. WGS reaction is a reaction in which carbon monoxide in syngas and water vapor react together to produce hydrogen and carbon dioxide [17]. Based on the reaction temperature range, it is divided into two categories: high-temperature water gas shift (HT-WGS) and low-temperature water gas shift (LT-WGS). The HT-WGS reaction takes place in the

range of $300 \sim 400\,^{\circ}\text{C}$, while the LT-WGS reaction is $200\sim300\,^{\circ}\text{C}$. Due to its exothermic nature, higher CO conversion is favorable for low temperatures [18,19]. Particularly, the LT-WGS reaction for hydrogen production from pet coke has a high concentration of CO_2 while going through the HT-WGS reaction [20]. Therefore, it is necessary to develop a catalyst to minimize the decrease in activity because a high concentration of CO_2 causes a decrease in the activity of the catalyst.

For LT-WGS conditions, Cu-based catalysts are being researched extensively because of their exothermic nature. Nevertheless, there are many shortcomings, such as-lower thermal stability, mechanical strengths, poisoning tolerance, and short lifetime [21-23]. Due to resolving these issues, Mg can be considered as assisting in enhancing the activity and thermal stability of active components. Hou et al. [24] and Zhang et al. [25] reported that the Mg^{2+} charge is similar to Cu^{2+}; an even closer ionic radius makes it a fascinating element. In addition, small amounts of MgO in the catalyst improve its activity and sustainability. Moreover, MgO can stabilize the Cu^+ active species and catalyze the WGS reaction between Cu^0 and Cu^+ by surface reduction-oxidation [26,27]. Various research has been conducted by using Mg in the catalyst. Park et al. [28] reported that Mg-containing $Cu/ZnO/MgO/Al_2O_3$ catalyst demonstrated higher catalytic activity than the catalyst without magnesium oxide (CZA) for LT-WGS. Nishida et al. [29] also found $Cu/Zn/Al_2O_3$ catalyst with high catalytic activity for WGS by doping a small amount of MgO. Thouchprasitchai et al. [22] also mentioned $Cu_{0.15}Mg_3Al$-CP300 catalyst synthesizing by co-precipitation method represented the lowest reduction temperature and the highest catalytic activity for WGS. Besides, research has been conducted extensively to modify a Cu-based for LT-WGS to improve the catalytic activity.

In this study, a catalyst was developed to prevent the deactivation of catalyst activity under high CO_2 conditions. We prepared various Mg-based Cu/Al catalysts with different molar ratios via the co-precipitation method and investigated the effect of aging time and temperature to evaluate the effect of catalytic activity. Several characterization methods were carried out, including XRD, N_2 adsorption-desorption, and H_2-TPR analysis. Moreover, the long-term catalytic activity was carried out at a fixed temperature of $300\,^{\circ}\text{C}$ that continued for 19 h.

2. Material and methods

2.1. Synthesis of CMA catalysts

The co-precipitation method was used to prepare $Cu/MgO/Al_2O_3$ samples with different molar ratios by using an aqueous solution of $Cu(NO_3)_2\cdot3H_2O$ ($99.0 \sim 105.0\%$, JUNSEI), $Mg(NO_3)_2\cdot6H_2O$ (99.0%, JUNSEI), and $Al(NO_3)_3\cdot9H_2O$ (98.0%, JUNSEI). The copper amount was fixed at 30 mol%, and Mg/Al varies. Na_2CO_3

(99.8%, JUNSEI) was used as precipitating agent, added 3 ml min^{-1} was put into a beaker containing nitrate solution under stirring at room temperature by a peristaltic pump. NaOH (97.0%, KANTO CHEMICAL) solution was added slowly dropwise to control pH (10 ± 0.2). After precipitation, the suspension was aged for 24, 48, and 72 h at 40, 60, and $80\,^{\circ}\text{C}$ with stirring. The resulting precipitate was filtered and washed three times with DI water and dried in an oven at $100\,^{\circ}\text{C}$ for 12 h. Finally, calcined at $500\,^{\circ}\text{C}$ for 5 h ($5\,^{\circ}\text{C}$ min^{-1}) in a static air atmosphere. Catalysts are referred to as CMA_molar ratio/aging temperature/aging time. For example, the CMA_334/60/24 catalyst has a Cu/Mg/Al molar ratio of 3:3:4, an aging temperature of $60\,^{\circ}\text{C}$, and a catalyst aged for 24 h.

2.2. Characterization

The crystalline structure of the catalysts was analyzed by X-ray Diffraction (Bruker D8 ADVANCE Powder) with Cu Kα1 (λ =1.54056 Å) at 40 kV and 40 mA. Scan speed $1\,^{\circ}\text{C}$ min^{-1}, scan step was 0.02, and 2 thetas range from 10 to 90 degrees. N_2 physical adsorption and desorption was conducted at 77.35 K by BELSORP-miniX (Microtrac BEL) instrument. The sample was degassed at $200\,^{\circ}\text{C}$ for 4 h under a vacuum before N_2 adsorption. The surface area, average pore diameter, and pore volume were calculated by the Brunauer-Emmett-Teller (BET) method. Temperature-programmed reduction by H_2 (H_2-TPR) analysis was performed on BELCAT-M (BEL Japan Inc.) instrument equipped with a thermal conductivity detector (TCD). Typically, around 50 mg of the sample was heated up to $500\,^{\circ}\text{C}$ at a ramping rate of $5\,^{\circ}\text{C}$ min^{-1} with the gas mixture of 10.03 vol.% H_2 balanced with Ar.

2.3. WGS reaction measurement

The catalytic evaluation experiment was performed with a fixed bed reactor at atmospheric pressure. A quartz reactor with an inner diameter of ¼ inch was used at a temperature range of 180~420 $^{\circ}\text{C}$. A thermocouple was installed inside the reactor to record the reaction temperature. Typically, a calcined catalyst was pelletized, sieved (150-300 μm) and placed in the reactor at 2 cm height. Before the WGS reaction, the catalysts were reduced under 50 vol% H_2/N_2 with the total gas flow rate of 80 cc min^{-1} at $300\,^{\circ}\text{C}$ for 1 h, and then the temperature decreased at the reaction condition. Water vapor was supplied by a mini chemical pump (NP-KX-200, Nihon Seimitsu Kagaku Co., Ltd). The reaction was started by introducing the gas mixture (10.01 vol.% CO, 55.02 vol.% H_2, 34.97 vol.% CO_2) to the reactor with a flow rate of 50 cc min^{-1} where the steam/CO ratio was 3. Output CO amount was analyzed by a gas chromatography (GC) (3000 Micro GC INFICON) system equipped with a thermal conductivity detector (TCD). Finally, the activity was checked for each temperature, and the CO conversion was calculated by the

following equation.

CO conversion = (mole of consumed CO/mole of input CO) × 100

For long-term experiments, all conditions were the same as the water gas shift reaction as mentioned previously by using the same reactor. The reactor temperature was fixed at 300 °C that continued for 19 h. The results were analyzed by gas chromatography, divided into 1 h units, and average values were obtained to compare conversion rates.

3. Results and Discussion

3.1. Effect of different molar ratio

The BET analysis results of CMA catalysts with different molar ratios are shown in Table 1. The surface area, average pore diameter, and pore volume of these catalysts have been mentioned. With increasing alumina, surface area rises. CuO peaks strengthened for the CMA_352/60/24 catalyst, confirmed by the results of XRD and H_2-TPR; as a result, the surface area was the lowest. On the other hand, the CMA_334/60/24 catalyst represents the highest surface area among these three catalysts. The N_2 adsorption-desorption isotherms for all CMA catalysts showed a type IV, in which capillary condensation is accompanied by hysteresis relating to mesoporous materials.

Figure 1 displays the X-ray diffraction (XRD) analysis of the crystallinity of CMA catalysts with different molar ratios. As

reported by Li et al. [23] and Kong et al. [30], for CMA_ 343/60/24 and CMA_334/60/24, there is no CuO tenorite or $CuAl_2O_4$ spinel peak found, indicating that well dispersion of CuO in the catalyst (2θ values obtained 36, 44, 63°). As opposed to when the Mg amount was 50 mol%, the CMA_ 352/60/24 catalyst contains both CuO and MgO, which means CuO doesn't disperse well in this catalyst because Mg^{2+} was completely replaced by Cu^{2+}. As the Mg concentration increased, CuO peaks became adversely strengthened, indicating the formation of larger CuO nanoparticles. This outcome confirmed that CuO species dispersion was favorable with the suitable addition of Mg. No $CuAl_2O_4$ spinel peak was also confirmed by H_2-TPR profiles (Figure 2). Therefore, Mg is required in sufficient amounts to promote the enhanced dispersion of the CuO species; we also agree on this point with Kong et al. [30] work.

Catalyst reduction profiles were determined by performing the H_2-TPR experiment in Figure 2. For all the CMA samples with different molar ratios mentioned, H_2 consumption was in the range of 200 ~ 250 ℃. The Gaussian distribution was used to split the hydrogen consumption peak range for well understanding of the TPR result, such as α, β, and γ peak. A single reduction peak was observed for CMA_343/60/24, indicating good Cu^{2+} dispersion. Converting CuO to copper metal is easily possible at lower reduction temperatures without affecting the catalyst's structure [31]. For other catalysts, the low-temperature peak was attributed to the reduction of well-dispersed copper species in CuO, and the high-temperature peak was associated with the reduction of bulky-like CuO phases [32-34]. Though CMA_ 334/60/24 catalyst shows a small CuO peak that we confirmed from the H_2-TPR result, it doesn't detect in the XRD result. However, we are unable to avoid the presence of small CuO particles due to the limitation of XRD measurement. In agreement with the XRD result of Figure 1, there was no detectable
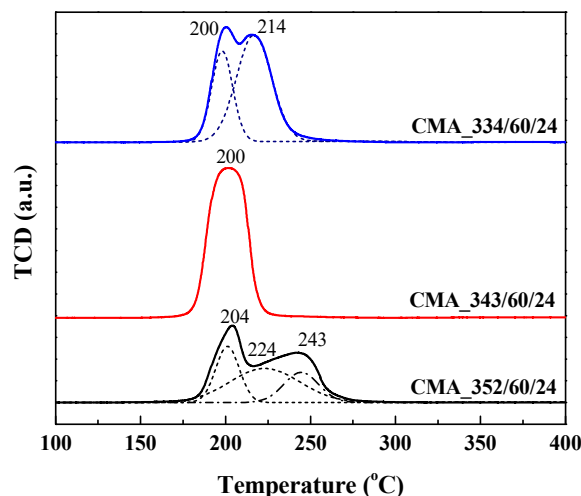
Table 1. BET analysis result of CMA catalysts with different molar ratio

Catalysts	Surface area [$m^2\ g^{-1}$]	Average pore diameter [nm]	Pore Volume [$cm^3\ g^{-1}$]
CMA_334/60/24	134	30.7	30.7
CMA_343/60/24	123	22.7	28.3
CMA_352/60/24	94	15.4	21.7

Figure 1. XRD patterns of CMA samples after calcination at 500 ℃.

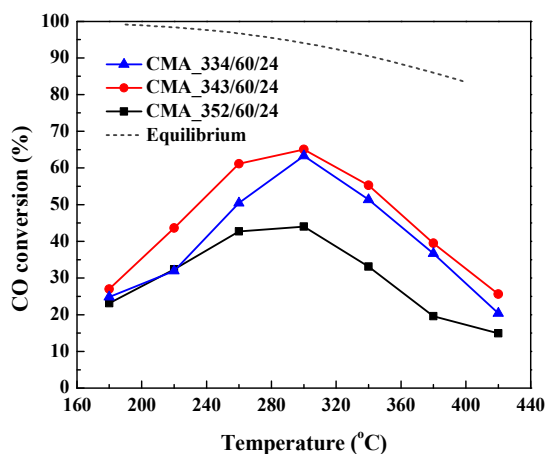**Figure 2.** H_2-TPR profiles of the CMA catalysts.

Figure 3. CO conversion of the CMA catalysts.

reduction peak that contributed to the $CuAl_2O_4$ spinel phase. The hydrogen reduction peak shifted to a higher temperature, increasing the Mg amount in the CMA catalyst for CMA_352/60/24 catalyst, indicating a greater interaction between copper species and the support material [35]. As a result, ease of reducibility and metal dispersion was most likely one of the most influential factors in determining catalytic activity. Consequently, only a suitable amount of Mg showed the lowest reduction temperature.

Figure 3 illustrates the CO conversion of the CMA catalysts with different molar ratios. Among the three catalysts, the CMA_343/60/24 demonstrated the highest catalytic activity, around 65%, with GHSV $14,089\,h^{-1}$, as it has the lowest reduction temperature evidenced by the H_2-TPR result [33]. In addition, side reactions did not occur in all catalysts under each reaction condition. Another important factor, the well dispersion of CuO, also assists in the improvement of the catalytic activity. Although the CMA _334/60/24 catalyst had the highest surface area and well dispersion of CuO in the XRD result, the H_2.TPR test confirmed the presence of CuO bulk phases, indicating that well dispersion did not take place. As a result, it showed lower catalytic activity at a lower temperature range than the CMA_ 343/60/24 catalyst due to the presence of small bulk like CuO. On the other side, CMA_352/60/24 showed the lowest CO conversion as the presence of bulk-like CuO phases due to the replacement of Mg^{2+} by Cu^{2+}, confirmed by the result of XRD [33]. Additionally, this catalyst exhibited the lowest surface area, and low catalytic activity is expected. As a result, suitable Mg amounts (40 mol%) provide good catalytic activity. Consequently, the ease of reducibility with no bulk like CuO phase was a key factor in determining the catalytic activity.

3.2. Effect of aging temperature and time

The BET analysis results of CMA catalysts with different aging time and temperature are shown in Table 2. When the

Table 2. BET analysis result of CMA catalysts with different aging time and temperature

	Catalysts	Surface area [$m^2\,g^{-1}$]	Average pore diameter [nm]	Pore volume [$cm^3\,g^{-1}$]
Aging temperature	CMA_343/40/24	71	20.7	16.4
	CMA_343/80/24	72	32.7	16.5
Aging Time	CMA_343/60/48	83	33.1	19.1
	CMA_343/60/72	90	21.6	20.6

aging temperature was more or less than 60 °C, the surface area and pore volume decreased compared to the CMA_343/60/24 catalyst, resulting in nearly identical surface area and pore volume. On the contrary, as aging increases by more than 24 h, BET surface area decreases. This finding suggests that long aging periods are associated with a decline in physical abilities and observed the lower surface area.

TPR profiles of CMA catalysts with different aging temperature and aging time are shown in Figure 4. For Figure 4(a), at different aging temperature, temperature below and above 60 °C are reduced at high temperature. CMA_343/40/24 and CMA_343/80/24 catalysts exhibit a higher reduction temperature range of 220-250 °C,
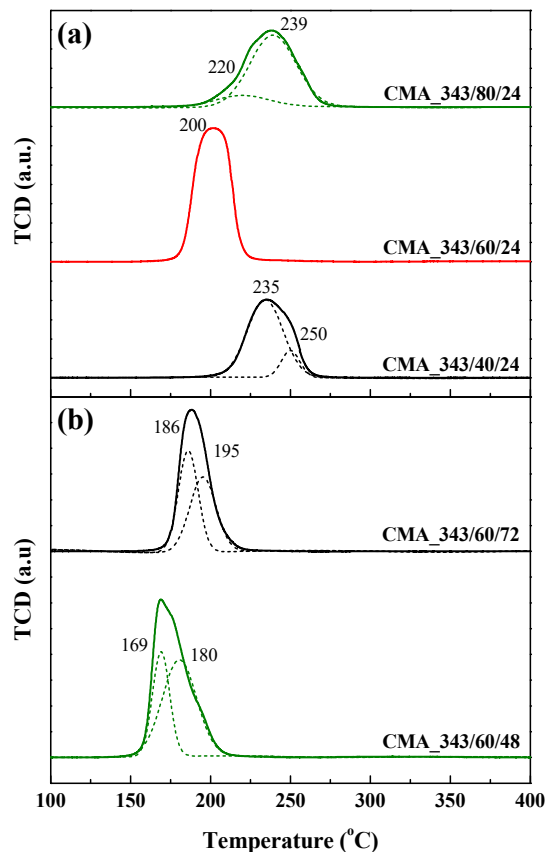

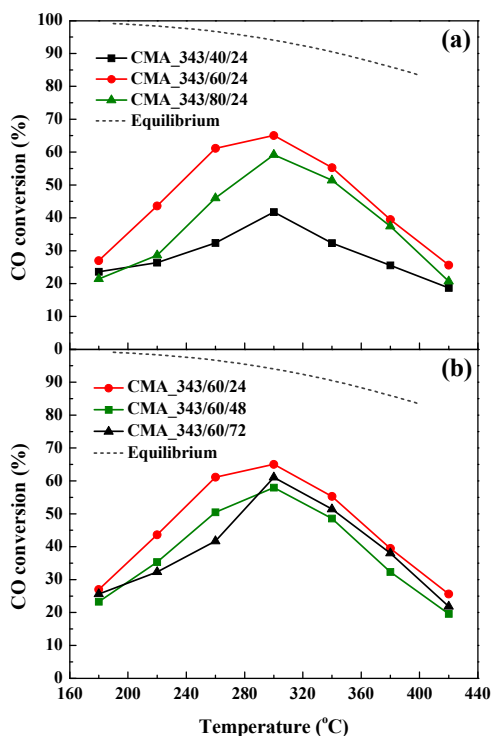**Figure 4.** H_2-TPR profiles of different catalysts (a) aging temperatures (b) aging times.

Figure 5. CO conversion of different catalysts (a) aging temperatures (b) aging times.

Figure 6. Long-term stability test for CMA_343/60/24 catalyst.

where a lower temperature peak is responsible for the high dispersion of CuO while higher temperature peak represents the bulk phase. A reduction occurs at high temperature, the surface area decreases, confirmed by nitrogen adsorption isotherm. In Figure 4(b), the peak shifted to a lower temperature with an increasing aging time of more than 24 h, but a small bulk-like CuO peak appeared due to the stepwise reduction of Cu^{+2} to Cu^0. Aging time has affected the formation of CuO species. The physical properties of the catalyst were strongly influenced by the aging temperature, which was also observed by Shim et al. [36].

Figure 5 shows the effect of aging temperature and aging time on CO conversion. For Figure 5(a), different aging temperatures below and above 60 °C negatively affect the CO conversion due to poor surface properties shown in Table 2. The most important thing is that high reduction temperature is also responsible for lower catalytic activity. On the other hand, increased aging time also influences catalytic activity, as shown in Figure 5(b). Catalysts that were aged for longer than 24 hours showed lower CO conversion. The CO conversion of the CMA_343/60/72 catalyst, which has been aged for a long time, is initially lower than that of the CMA_343/60/48 catalyst but represented slightly higher after 300 °C. Increasing the duration of aging is probably unfavorable for low temperatures, which represented the 72 h aged sample initially has a low CO conversion. Enhancing the catalytic activity requires not only the lowest reduction temperature but also a well-dispersed CuO
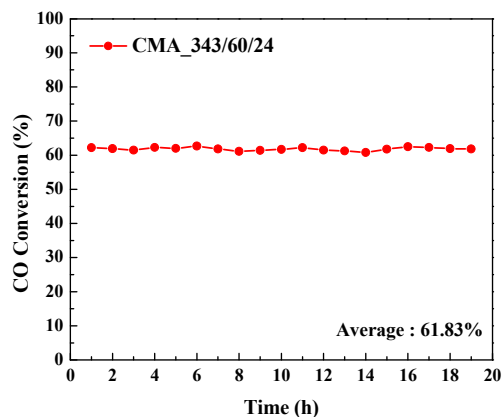
phase. It observed that well dispersion does not occur in the modified samples and resulting in low catalytic activity. Therefore, the ease of reducibility with no bulk like CuO phase was likely to be one of the essential factors in determining the catalytic activity [37].

3.3. Long-term operation

A long-term operation test of the optimal catalyst was performed to confirm the process's applicability. Figure 6 depicts the long-term stability of the CMA_343/60/24 catalyst at 300 °C for 19 h. Usually, the catalytic stability decreased with time during the long-term stability test. This work observed that the CMA_343/60/24 catalyst maintained a constant average CO conversion rate of 61.83% for 19 h without much deactivation under CO_2-rich feed gas. Since CO_2 is produced during the WGS reaction, a higher concentration of CO_2 in the feed gas decreases the conversion of CO [38]. Although the outcome of the steady-state stability test for 19 h was unsatisfactory, it was confirmed that it maintained the stable catalytic activity under high CO_2 concentration conditions. Accordingly, it can be suggested that the possibility of applying the WGS process as CMA_343/60/24 catalyst prevents the degradation of catalyst activity when exposed to high CO_2 conditions feed gas.

4. Conclusions

This work investigated the effect of Mg and extended with different aging times and temperatures by synthesizing Cu/MgO/Al₂O₃ samples via the co-precipitation method. Among all catalysts prepared in this research, the highest activity was obtained for CMA_343/60/24 catalyst around 65% at 300 ℃ optimum temperature due to the lowest reduction temperature with well dispersion of CuO. However, the higher Mg containing CMA_352/60/24 catalyst represented the lowest CO conversion because CuO wasn't properly dispersed. This finding

confirmed that only 40 mol% Mg provides better metal dispersion of the catalyst, which plays a vital role in improving catalytic activity. On the other side, the aging temperature of more or less than 60 °C had lower catalytic activity due to poor surface area, as they are reduced at a higher temperature with the presence of bulk CuO species. In contrast, despite having the lower reduction temperature for catalysts with increasing aging time represented lower CO conversion due to the presence of bulk CuO species. Interestingly, it can be concluded that 6 °C aging temperature and 24 h aging time are ideal for excellent catalytic activity. In terms of catalyst stability, CMA_343/60/24 catalyst has no detectable deactivation that proved good catalytic stability under high CO_2 concentration. The catalyst remained stable at each temperature and long-term stability test, which will help prevent catalyst deactivation even under conditions of high CO_2 concentration.

Acknowledgement

References

1. Johnston, B., Mayo, M. C., and Khare, A. "Hydrogen: The energy source for the 21st century," *Technovation*, **25**(6), 569-585 (2005).

2. Karayel, G. K., Javani, N., and Dincer, I., "Green hydrogen production potential for Turkey with solar energy," *Int. J. Hydrog. Energy*, **47**(45), 19354-19364 (2022).

3. Buffi, M., Prussi, M., and Scarlat, N., "Energy and environmental assessment of hydrogen from biomass sources: Challenges and perspectives," *Biomass Bioenerg*, **165**, 106556 (2022).

4. Hermesmann M., and Müller, T. E., "Green, Turquoise, Blue, or Grey? Environmentally friendly Hydrogen Production in Transforming Energy Systems," *Prog. Energy Combust. Sci.*, **90**, 100996 (2022).

5. Dawood, F., Anda, M., and Shafiullah, G. M., "Hydrogen production for energy: An overview," *Int. J. Hydrog. Energy*, **45**(7), 3847-3869 (2020).

6. Qureshi, F., Yusuf, M., Kamyab, H., Vo,. D. V., Chelliapan, S., Joo, S. W., Vasseghian, Y., "Latest eco-friendly avenues on hydrogen production towards a circular bioeconomy: Currents challenges, innovative insights, and future perspectives," *Renew. Sust. Energ. Rev.*, **168**, 112916 (2022).

7. Yu, M., Wang, K. and Vredenburg, H., "Insights into low-carbon hydrogen production methods: Green, blue and aqua hydrogen," *Int. J. Hydrog. Energy*, **46**(41), 21261-21273 (2021).

8. Wu, Y., Liu, F., He, J., Wu, M. and Ke, Y., "Obstacle identification, analysis and solutions of hydrogen fuel cell vehicles for application in China under the carbon neutrality target," *Energy Policy*, **159**, 112643 (2021).

9. Sadik-Zada, E. R., "Political economy of green hydrogen rollout: A global perspective," *Sustain.*, **13**(23), 13464 (2021).

10. Oni, A. O., Anaya, K., Giwa, T., Di Lullo, G., and Kumar, A., "Comparative assessment of blue hydrogen from steam methane reforming, autothermal reforming, and natural gas decomposition technologies for natural gas-producing regions," *Energy Convers. Manag.*, **254**, 115245 (2022).

11. Park, J. H., Hong, M. W., and Yi, K. B., "Reaction Characteristics of Water Gas Shift Catalysts in Various Operation Conditions of Blue Hydrogen Production Using Petroleum Cokes," *Clean Technol.*, **28**(1), 1-8 (2022).

12. Wang, M.,Wan, Y., Guo, Q., Bai, Y., Yu, G., Liu, Y., Zhang, H., Zhang, S., Wei, J., "Brief review on petroleum coke and biomass/coal co-gasification: Syngas production, reactivity characteristics, and synergy behavior," *Fuel*, **304**, 121517 (2021).

13. Ba, Z., Zhao, J., Li, C., Huang, J., Fang,. Y., Zhang, L., Kong, L., Wang, Q., "Developing efficient gasification technology for high-sulfur petroleum coke to hydrogen-rich syngas production," *Fuel*, **267**, 117170 (2020).

14. Murthy, B. N., Sawarkar, A. N., Deshmukh, N. A., Mathew, T. and Joshi, J. B "Petroleum coke gasification: A review," *Can. J. Chem. Eng.*, **92**(3), 441-468 (2014).

15. Ilieva L., Lvanov, l., Petrova, P., Munteanu, G., Karakirova, Y., Sobczak, J. W., Lisowski, W., Anghel, E. M., Kaszkur, Z., and Tabakova, T., "Effect of Y-doping on the catalytic properties of CuO/CeO₂ catalysts for water-gas shift reaction," *Int. J. Hydrog. Energy*, **45**(49), 26286-26299 (2020).

16. Pal, D. B., Chand, R., Upadhyay, S. N., and Mishra, P. K., "Performance of water gas shift reaction catalysts: A review," *Renew. Sust. Energy Rev.*, **93**, 549-565 (2018).

17. Ebrahimi, P., Kumar, A., and Khraisheh, M., "A review of recent advances in water-gas shift catalysis for hydrogen production," *Emergent Mater.*, **3**(6), 881-917 (2020).

18. Jeong, C. H., Byeon, H. J., Jang, W. J., Jeon, K. W., and Jeong, D. W. "The optimization of Nb loading amount over Cu–Nb–CeO₂ catalysts for hydrogen production via the low-temperature water gas shift reaction," *Int. J. Hydrog. Energy*, **45**(16), 9648-9657 (2020).

19. Baraj, E., Ciahotný, K., and Hlinčík, T., "The water gas shift reaction: Catalysts and reaction mechanism," *Fuel*, **288**, 119817 (2021).

20. Pradhan, S., Reddy, A. S., Devi, R. N., and Chilukuri, S. "Copper-based catalysts for water gas shift reaction: Influence of support on their catalytic activity," *Catal. Today*, **141**(1-2), 72–76 (2009).

21. Ay, S., Ozdemir, M., and Melikoglu, M., "Effects of magnesium and chromium addition on stability, activity and structure of copper-based methanol synthesis catalysts," *Int. J. Hydrog.*

Energy, **46**(24), 12857-12873 (2021).

22. Thouchprasitchai, N., Luengnaruemitchai, A., and Pongstabodee, S., "The activities of Cu-based Mg-Al layered double oxide catalysts in the water gas shift reaction," *Int. J. Hydrog. Energy*, **41**(32), 14147-14159 (2016).

23. Li, D., Cai, Y., Chen, C., Lin, X., and Jiang, L. "Magnesium-aluminum mixed metal oxide supported copper nanoparticles as catalysts for water-gas shift reaction," *Fuel*, **184**, 382-389 (2016).

24. Hou, X., Qing, S., Liu, Y., Li, L., Gao, Z., and Qin, Y., "Enhancing effect of MgO modification of Cu–Al spinel oxide catalyst for methanol steam reforming," *Int. J. Hydrog. Energy*, **45**(1), 477-489 (2020).

25. Zhang F., Zhan, Y., Liu, Y., Gasem, K. A. M., Chen, J., Chiang, F., Wang, Y., Fan, M., "Synthesis of Cu/Zn/Al/Mg catalysts on methanol production by different precipitation methods," *Mol. Catal.*, **441**, 190-198 (2017).

26. Shishido, T., Yamamoto, M., Atake, I., Li, D., Tian, Y., Morioka, h., Honda, M., Sano, T., and Takehira, K., "Cu/Zn-based catalysts improved by adding magnesium for water–gas shift reaction", *J Mol. Catal. A Chem.*, **253**(1-2), 270-278 (2006).

27. Shishido, T., Yamamoto, M., Li, D., Tian, Y., Morioka, H., Honda, M., Sano, T., Takehira, K., "Water-gas shift reaction over Cu/ZnO and Cu/ZnO/Al₂O₃ catalysts prepared by homogeneous precipitation," *Appl. Catal. A Gen.*, **303**(1), 62-71 (2006).

28. Park, J. H., Baek, J. H., Hwang, R. H., and Yi, K. B., "Enhanced Catalytic Activity of Cu/ZnO/Al₂O₃ Catalyst by Mg Addition for Water Gas Shift Reaction," *Clean Technol.*, **23**(4), 429-434 (2017).

29. Nishida. K., Li, D., Zhan, Y., shishido, T., Oumi, Y., Sano, T., Takehira, K., "Effective MgO surface doping of Cu/Zn/Al oxides as water-gas shift catalysts," *Appl. Clay Sci.*, **44**(3-4), 211-217 (2009).

30. Kong, X., Chen, Z., Wu, Y., Wang, R., Chen, J., and Ding, L. "Synthesis of Cu-Mg/ZnO catalysts and catalysis in dimethyl oxalate hydrogenation to ethylene glycol: Enhanced catalytic behavior in the presence of a Mg²⁺ dopant," *RSC Adv.*, **7**(78), 49548-49561 (2017).

31. Asthana, S., Samanta, C., Bhaumik, A., Banerjee, B., Voolapalli, R. K., and Saha, B., "Direct synthesis of dimethyl ether from syngas over Cu-based catalysts: Enhanced selectivity in the presence of MgO," *J. Catal.*, **334**, 89-101 (2016).

32. Sharma S. K. Paul, B., Bhanja, P., Poddar, M. K., Samanta, C., Khan, T. S., Haider, M. A., Bal, D. R., "Understanding the Origin of Structure Sensitivity in Nano Crystalline Mixed Cu/Mg−Al Oxides Catalyst for Low-Pressure Methanol Synthesis," *ChemCatChem*, **13**(14), 3290-3302 (2021).

33. Jia, M. L., Zhang, Y. P., Bao, Y. S., Wang, J., and Xu, A. J., "Recyclable CuMgAl hydrotalcite for oxidative esterification of aldehydes with alkylbenzenes," *Green Chem. Lett. Rev.*, **11**(3), 230-236 (2018).

34. Cheng Z., Zhou, W., Lan, G., Sun, X., Wang, X., Jiang, C., Li, Y., "High-performance Cu/ZnO/Al₂O₃ catalysts for methanol steam reforming with enhanced Cu-ZnO synergy effect via magnesium assisted strategy," *J. Energy Chem.*, **63**, 550-557 (2021).

35. Everbroeck, V. T., Papavasiliou, A., Ciocarlan, R. G., Poulakis, E., Philippopoulos, C. J., Jardim, E. O., Albero, J. S., Sakellis, E., Cool, P., Katsaros, F. K., "Towards Highly Loaded and Finely Dispersed CuO Catalysts via ADP: Effect of the Alumina Support," *Catalysts*, **12**(6), 628 (2022).

36. Shim, J. O., Na, H. S., Ahn ,S. Y., Jeon, K.W., Jang, W. J., Jeon, B.H., Roh, H.S., "An important parameter for synthesis of Al₂O₃ supported Cu-Zn catalysts in low-temperature water-gas shift reaction under practical reaction condition," *Int. J. Hydrog. Energy*, **44**(29), 14853-14860 (2019).

37. Zhang L., pan, L. W., Ni, C. J., Sun, T. J., Wang, S. D., Hu, Y. K., Wang, A.J., Zhao, S.S., "Effects of precipitation aging time on the performance of CuO/ZnO/CeO₂-ZrO₂ for methanol steam reforming," *J. Fuel Chem. Technol.*, **41**(7), 883-888 (2013).

38. Meng, F., Li, X., Lv, X., and Li, Z., "CO hydrogenation combined with water-gas-shift reaction for synthetic natural gas production: a thermodynamic and experimental study," *Int. J. Coal Sci. Technol.*, **5**(4), 439-451 (2018).